Published in final edited form as:
Biochemistry. 2013 April 16; 52(15): 2649–2654. doi:10.1021/bi301638h.

Lipid-Induced Conformational Changes within the Cytochrome b_6f Complex of Oxygenic Photosynthesis

S. Saif Hasan[*], **Jason T. Stofleth**[*,#], **Eiki Yamashita**[&], and **William A. Cramer**[*,†]

[*]Department of Biological Sciences, Purdue University, West Lafayette IN 47907, USA

[#]Department of Chemistry and Biochemistry, University of California, San Diego CA 92037, USA

[&]Institute for Protein Research, Osaka University, Osaka, Japan

Abstract

Cytochrome b_6f catalyzes quinone redox reactions within photosynthetic membranes to generate a transmembrane proton electrochemical gradient for ATP synthesis. A key step involves electron transfer from the [2Fe-2S] cluster of the iron-sulfur protein (ISP) extrinsic domain to the cytochrome *f* heme across a distance of 26 Å, which is too large for competent electron transfer, but which could be bridged by translation-rotation of the ISP. Here we report the first crystallographic evidence for significant motion of the ISP extrinsic domain. It is inferred that extensive crystallographic disorder of the ISP extrinsic domain indicates conformational flexibility. The ISP disorder observed in the present structure, in contrast to the largely ordered ISP structure observed in the b_6f complex supplemented with neutral lipids, is attributed to electrostatic interactions arising from anionic lipids.

Keywords

Cytochrome *bc* complexes; electron transfer; anionic lipid

Introduction

The cytochrome b_6f complex (cyt b_6f) (Fig. 1) of oxygenic photosynthesis, along with the cytochrome bc_1 complex in the respiratory chain and purple photosynthetic bacteria, belongs to the hetero-oligomeric family of transmembrane cytochrome *bc* complexes, (1, 2). Cyt *bc* complexes share extensive structural and functional homology (2–5). Together, these complexes catalyze proton-coupled electron transfer reactions of the substrate quinone/-ol to generate a transmembrane proton electrochemical gradient that is utilized for ATP synthesis (5). On the electrochemically positive (p) side of the membrane, an electron is transferred from the substrate quinol, bound within the transmembrane p-side quinol oxidation (Q_p) site, to the [2Fe-2S] cluster of the iron-sulfur protein (ISP) extrinsic domain. The electron is then

[†]waclab@purdue.edu, Phone: 765-494-4956.

Supplementary Information. Crystals of the cyt b_6f complex from *M. laminosus* obtained in the presence of the anionic lipid DOPG. Crystal morphology is different from that observed previously for *M. laminosus* cyt b_6f crystals supplemented with the neutral lipid DOPC. This material is available free of charge via the Internet at http://pubs.acs.org.

transferred to the extrinsic heme *f* or c_1, respectively, in the b_6f or bc_1 complex, where it is utilized for the reduction of $NADP^+$ and O_2.

Crystal structures of the cyt b_6f complex show that the ISP [2Fe-2S] cluster is separated from the extrinsic heme *f* by ca. 26 Å (6–10). Direct transfer of electrons from the [2Fe-2S] cluster to heme *f* would then be expected to proceed at a rate that is orders of magnitude slower than required physiologically (11). In the cyt bc_1 complex, electron transfer rates are accelerated by a large-scale domain motion of the ISP extrinsic domain that bridges the distance to the heme of cyt c_1 (12). Based on the homology between cyt *bc* complexes, it is expected that the cyt b_6f ISP extrinsic domain must also undergo conformational changes to transfer electrons from the membrane extrinsic quinol to the cyt *f* heme (4, 6). However, crystal structures of the cyt b_6f complex obtained in the presence of quinone analog inhibitors have thus far not revealed evidence of large-scale changes in the position of the ISP extrinsic domain (6, 7, 9, 10). Although cyt *f* in the b_6f complex and cyt c_1 of the bc_1 complex each act as the electron acceptor for the [2Fe-2S] cluster in the ISP extrinsic domain, the structure of the extrinsic domains of cyt *f* and cyt c_1 is not conserved and is markedly different (13, 14). The extrinsic domain of cyt *f* consists of a 75 Å elongated β–sheet (Fig. 2A) while the cyt c_1 extrinsic domain is more compact and predominantly α-helical (Fig. 2B). Therefore, the structural barrier provided by the extrinsic domain of cyt *f* and cyt c_1 to motion of the ISP extrinsic domain is different (6, 15). The elongated structure of the cyt *f* extrinsic domain restricts the space available for ISP conformational changes, which are required to move the [2Fe-2S] cluster of the ISP extrinsic domain from a membrane proximal location to a cyt *f* proximal position. Neither the nature of conformational changes undergone by the ISP extrinsic domain during electron transfer by the b_6f complex nor the local driving force for the redox-linked conformational change is known. Hence, understanding of redox-linked ISP conformational changes within the cyt b_6f complex has remained relatively limited. Utilizing a new 2.80 Å crystal structure of the cyt b_6f complex isolated from the moderately thermophilic filamentous cyanobacterium *Mastigocladus laminosus* (PDB ID 4I7Z), we present evidence for extrinsic domain flexibility of the ISP in the b_6f complex.

Materials and Methods

Protein Purification

Mastigocladus laminosus thylakoid membranes were prepared as described previously (16, 17). Cyt b_6f was purified from the membranes with minor modifications to the purification protocol. Briefly, after β-octyl-glucoside (Anatrace) and sodium cholate (Sigma-Aldrich) mediated extraction of the protein from thylakoid membranes, and partial purification by ammonium sulfate precipitation and hydrophobic interaction chromatography using a propyl-agarose resin, the protein eluted from the hydrophobic column was concentrated to 4.8 ml and loaded on six sucrose density gradient tubes (~10 ml per tube of 10–32% sucrose in Tris-HCl, 30mM, pH 7.5 at 4°C, NaCl 50 mM, $MgCl_2$ 5 mM, KCl 5 mM, EDTA 1 mM, 6-amino-caproic acid and benzamidine 6 mM, 0.05% UDM (Anatrace, solubility-grade)). Following two sucrose density gradient centrifugation steps (16 hours, 36,000 × rpm (SW-41 rotor, Beckman), 4°C), pure cyt b_6f dimer was pooled and concentrated in an

Amicon-4 concentrator (100,000 nominal molecular weight cut-off) to ~200 μL. The protein buffer was exchanged to Tris-HCl 30 mM, pH 7.5 (pH equilibrated at room temperature, ~25°C), NaCl 50 mM, sucrose 10% and analytical grade UDM (Anatrace) 0.05% (TNS-UDM buffer) at 4°C. The buffer was then exchanged to TNS and 0.15% UDM supplemented with 1.8 mM DOPG. The protein was concentrated to 135–180 μM. The DOPG containing buffer for protein crystallization was prepared from a DOPG lipid stock (25 mg/ml, Avanti Polar Lipids) in organic solvent. 200 μL of the lipid was dried in a glass test-tube under a nitrogen stream and then left overnight in a dessicator. The dried lipid was suspended in the TNS buffer by gentle vortexing. Analytical grade UDM (Anatrace) was added to a final concentration of 0.15% (weight/volume), and the buffer was frozen and thawed in liquid nitrogen 15 times. The clarified buffer containing the DOPG lipid was then sonicated in a water bath (20 min, room temperature). The buffer (1.8 mM DOPG) was cooled to 4°C prior to protein buffer exchange.

Protein Crystallization and Cryo-freezing

Cyt b_6f was crystallized as described previously (10), with minor modifications. Briefly, 1.5 μL of the protein (135–180 uM) was mixed with an equal volume of the reservoir solution (Tris-HCl, 100 mM, pH 8.5 at room temperature, $MgCl_2$ 200 mM, $CdCl_2$ 40 mM and PEG-550 MME 16–17%) at 4°C. Hexagonal bipyramidal crystals appeared in 24–36 hours at 4°C through hanging drop vapor diffusion and grew to a size of 100–150 μm in the largest dimension (Supplementary Information, Fig. S1). For cryo-protection, after 5–7 days, crystals harvested from the 16% PEG 550 MME droplet were transferred to a cryo-protection buffer (500 μL of Tris-HCl 100 mM, pH 8.5 (pH equilibrated at room temperature), $MgCl_2$ 200 mM, $CdCl_2$ 40 mM, PEG 550 MME 21%, UDM 0.15% (Analytical-grade), 0.18 mM DOPG) in a sealed chamber for 30 minutes at 4°C. 250 uL of the buffer was then removed and replaced by an equal volume of the same buffer supplemented with 5% glycerol. The glycerol concentration was increased gradually to 25%, after which the crystals were flash-frozen in liquid nitrogen.

X-Ray Data-Collection, Data Reduction, Structure Solution

Diffraction data sets were collected under cryo-conditions (100 K) at beam line 23-ID-B, Advanced Photon Source, Argonne (IL), USA. Data reduction and scaling were performed in the HKL2000 suite (18) to $\langle I \rangle / \langle \sigma_I \rangle \approx 2$ in the highest resolution shell. Negative reflections were omitted during scaling. Diffraction data sets from two crystals were merged together to increase completeness. Rigid body refinement was performed in REFMAC5 (19), using an initial monomeric polypeptide model of the *M. laminosus* cyt b_6f complex (PDB ID 2E74) (10). Prosthetic groups, lipids, detergents, and water molecules were built into the structure using Coot (20) followed by several cycles of restrained refinement in REFMAC5 and Phenix (21). Table 1 summarizes the crystallographic structure statistics. Coordinates have been deposited in the Protein Data Bank with the PDB ID 4I7Z.

Structural Superposition

Coordinates of cyt b_6f crystal structures (PDB ID 2E74, 2E76 and 4I7Z) were superposed in PyMol (www.pymol.org). Fitting was performed using a pair-fit routine between the

backbone C_α atoms of the cyt b_6 subunit (chain A) of PDB ID 2E76 and 2E74 (Cα root mean squared deviation=0.41 Å), and between 2E76 and 4I7Z (C_α root mean squared deviation=0.42 Å).

Identification of the ISP Docking Interface

Coordinates of the cyt b_6f structure (PDB ID 2E76) obtained in the presence of the quinone analog inhibitor tridecyl-stigmatellin were analyzed with the Ligand-Protein Server (22). An interaction distance cut-off of 4.0 Å was imposed to identify the ISP extrinsic domain residues (chain D, residues 109–179) that interact with the transmembrane ISP binding site formed by cytochrome b_6 (chain A, residues Trp146, Lys149, Ile150 and Val154) and subunit IV (chain B, Phe69, Thr71, Pro72, Leu73, Ile75, Phe85, Leu88, Arg89, Lys94, Leu151). ISP extrinsic domain residues Thr109, His110, Leu111, Gly112, Cys113, Val114, Pro127, Cys128, His129 and Pro145 make contact with the residues of cyt b_6 and sub IV.

Denaturing Electrophoresis

Purification of cyt b_6f from spinach thylakoid membranes and SDS-PAGE analysis was performed as described (23). The purified protein was concentrated to 90 μM in the presence of Tris-HCl (100 mM, pH 7.5), NaCl (50 mM) and lipid (900 μM DOPG or DOPC, Avanti Polar Lipids). 10 μg protein loaded in each well was separated by electrophoresis using a current of 12.5–15.0 milli-Amperes.

Results

Purified, delipidated *M. laminosus* cyt b_6f complex was co-crystallized with the physiological anionic lipid dioleoylphosphatidylglycerol (DOPG). Previous crystal structures of the cyt b_6f complex were obtained in the presence of either the synthetic neutral lipid dioleoylphosphatidylcholine (DOPC) (6, 9, 10) or native lipids (7), which are predominantly neutral electrostatically (24, 25) and have been found to be associated with an ordered ISP extrinsic domain. Unit cell parameters ($P6_122$, a=b=159.45 Å, c=362.75 Å, α=β=90, γ=120) of the structure reported in the present study were similar to those reported earlier for the *M. laminosus* cyt b_6f structure (PDB ID 2E74, $P6_122$, a=b=158.34 Å, c=361.09 Å, α=β=90, γ=120) obtained in the presence of the neutral lipid DOPC (10). Electron density was assigned to seven of the eight polypeptide subunits within the b_6f monomer, which constitute the crystallographic asymmetric unit of the DOPG containing b_6f structure, with the exception of the ISP extrinsic domain. Electron density for the ISP was found to be incomplete beyond the p-side Ser46 residue of the ISP transmembrane helix (TMH).

A crystallographic structure analysis was performed to study the effect of lipid charge on the transmembrane docking surface for the ISP extrinsic domain. In the cyt bc_1 complex, transmembrane residues proximal to the Q_p-site that form the ISP docking interface have been reported to undergo conformational changes upon binding of the ISP extrinsic domain (26). The cyt b_6f ISP extrinsic domain is crystallographically defined in the presence of the neutral lipid DOPC in cyt b_6f structures obtained in the absence (PDB ID 2E74, resolution 3.00 Å) (10) and presence (PDB ID 2E76, resolution 3.43 Å) (10) of the quinone analog

inhibitor tridecyl-stigmatellin (TDS). In the presence of TDS, the ISP extrinsic domain is located closer to the transmembrane docking surface by approximately 3 Å (4). It was found in the present study that residues Thr109-Val114, Pro127-His129 and Pro145 of the ISP extrinsic domain (PDB ID 2E76) interact with the docking surface formed by the transmembrane cytochrome b_6 (cyt b_6) and subunit IV (sub IV) polypeptides (shown in Fig. 3). Conformational changes within the surface for ISP docking are not detected by superposition of the DOPG containing cyt b_6f structure with the cyt b_6f structure obtained with the neutral lipid DOPC (PDB ID 2E74, 2E76), in contrast with cyt bc_1 where changes in the cyt *b* interface for ISP docking have been documented (26).

The absence of detectable conformational changes in the ISP binding site of cyt b_6f in the presence of DOPC and DOPG raises the possibility that electrostatic interactions arising from lipid head group charge may cause conformational changes in the ISP extrinsic domain. The cyt b_6f crystal structure described in the present study has revealed four lipid sites per monomer (Fig. 4A). One natural acidic sulquinovosyldiacylglycerol (SQDG) molecule has been previously described on the electrochemically negative (n) side of the b_6f complex (7, 9, 10, 27). The SQDG lipid is involved in the stabilization of the ISP and cyt *f* TMH (28). Three additional lipids were identified in the present study and have been modeled as the acidic phosphatidylglycerol (PG). Two of the lipid sites have been described for the neutral lipid in the crystal structures of the cyanobacterial cyt b_6f complex (9, 10). The anionic PG lipid (“PG1”) occupies an n-side niche between the F and G TMH of sub IV (Fig. 4B). The lipid in this site was modeled as a DOPC in previous b_6f structures (9, 10). A p-side lipid binding site is formed by the peripheral Pet subunits G, L, M and N (Fig. 4C), which overlaps with the DOPC binding site in the cyanobacterial cyt b_6f complex (PDB IDs 2E74, 2ZT9) (9, 10). The PG lipid (“PG2”) also overlaps with the natural monogalactosyldiacylglycerol (MGDG) lipid found in the cyt b_6f structure obtained from *Chlamydomonas reinhardtii* (PDB ID 1Q90) (7).

A novel PG site (“PG3”) is located on the p-side between the ISP and cyt *f* TMHs (Fig. 4D). The ligand in this site was modeled as a detergent molecule in previously published cyanobacterial cyt b_6f crystal structures (PDB IDs 2E74, 2ZT9) (9, 10), and as the photosynthetic pigment eicosane in the *C. reinhardtii* cyt b_6f structure (7). This lipid binding site shows conservation of location with the yeast respiratory cyt bc_1 complex (PDB ID 3CX5). An anionic phosphatidic acid (PA) lipid occupies a similar site in the cyt bc_1 complex (29). It has been suggested that PA stabilizes the ISP TMH, while the extrinsic domain undergoes motion during catalysis (30). This lipid-occupied site may be directly involved in lipid mediated modulation of enzymatic activity in cyt *bc* complexes.

The thylakoid membrane consists predominantly of neutral lipids (24, 25). Anionic lipids form only a minor component and are restricted to the n-side leaflet of the thylakoid membrane bilayer (25). In an environment of predominantly anionic lipids, as provided in the crystallization solution, stability of the cyt b_6f complex may be affected, leading to the loss of the ISP extrinsic domain. Under such experimental conditions, the incomplete density of the ISP extrinsic domain can be attributed to secondary factors other than crystallographic disorder, such as proteolysis. To test the effect of anionic lipids on the stability of the cyt b_6f complex, a denaturing SDS-PAGE analysis was performed. The four

"large" subunits of the cyt b_6f complex, *i. e*., cyt *f*, cyt b_6, ISP and sub IV, do not show any shift in effective molecular weight (M_r) in the presence of the anionic lipid DOPG compared to the M_r of subunits observed in the presence of the neutral lipid DOPC (Fig. 5). It is inferred that the ISP subunit is stable upon interaction with DOPG.

Discussion

Examples of functions or structural roles of anionic lipids in the structure and function of membrane proteins have been documented and discussed (30, 31). The SQDG molecule in cyt b_6f has been shown to be involved in assembly and stability (28). In the Photosystem-II complex, SQDG contributes to biological activity (32–34). Mutants that lack SQDG demonstrate normal content of Photosystem-II, but with reduced activity that is restored by the addition of exogenous SQDG (33). Similarly, a PG molecule may participate directly in modulating kinetics of the bifurcated electron transfer pathway within the Photosystem-I complex (35, 36). In the cyt b_6f structure described here, while none of the four lipid binding sites comes in direct contact with the ISP extrinsic domain, the absence of a well-defined electron density for this domain in the anionic lipid environment indicates that the electrostatic influence of the charge on the lipid head group may be involved in the binding of the ISP extrinsic domain at the p-side transmembrane docking site. The dielectric constant of the environment around the acidic lipids on the p-side, and the ISP extrinsic domain docking site is expected to be much lower (37) than the bulk water dielectric constant of 81, which would permit the propagation of electrostatic interactions that alter ISP binding properties of the docking surface and the ISP extrinsic domain itself. Perhaps due to limitations of resolution (2.80–3.43 Å), such conformational changes have not been detected.

Conformational flexibility of the cyt b_6f ISP subunit has been a subject of debate. Mutagenesis of the ISP flexible hinge showed that the ISP is less susceptible to mutagenesis in the cyt b_6f than bc_1 (28, 38). This may be a consequence of the larger flexibility of the poly-glycine hinge in the cyt b_6f complex than of the poly-alanine hinge in bc_1. The hinge region is crystallographically disordered in the b_6f complex (9, 10), while its electron density is traced in the bc_1 complex (for example, in (39)), thereby indicating larger flexibility of the ISP extrinsic domain in the b_6f complex. In the presence of the neutral lipid DOPC, the cyt b_6f ISP extrinsic domain is docked proximal to the transmembrane segment (9, 10). From the present study, it is suggested that conformational flexibility of the ISP is a function of the lipid environment. Neutral and anionic lipids may be involved in modulating the extent of motion of the ISP extrinsic domain. From the b_6f structures obtained with the neutral lipid DOPC (9, 10), it is inferred that the ISP extrinsic domain *in-situ* is tethered in a membrane proximal position.

It is significant to note that thylakoid membrane anionic lipids are predominantly restricted to the n-side leaflet (25). The sidedness of lipids in crystal structures of photosynthetic membrane protein complexes follows their distribution in membranes (30). A tightly bound PG molecule has been identified in the purified cyt b_6f although the lipid is not observed in crystal structures (27). Since the ISP extrinsic domain is located on the p-side, it is important to note the possibility of transmembrane communication between an n-side lipid and the

membrane bound ISP extrinsic domain through the low dielectric transmembrane domain of the cyt b_6f complex. Further insights into lipid-induced conformational changes will be derived in the future from cyt b_6f crystal structures obtained at higher resolution.

Supplementary Material

Refer to Web version on PubMed Central for supplementary material.

Acknowledgments

We thank P. Afonine, R. Agarwal, J. T. Bolin, S. Kumar, P. Plevka, C. B. Post, V. M. Prasad, M. G. Rossmann, S. Savikhin and T. Schmidt for discussions, S. Corcoran (APS Beamline 23-ID-B), J. Chen and M. Oldham (Purdue U.) for advice on diffraction data collection and the CCP4 workshop 2010 for advice on structure solution.

Financial support was provided by National Institutes of Health grant GM-038323 and the Henry Koffler Distinguished Professorship (W.A.C.), and the Purdue University (S.S.H.).

Abbreviations

β-Car	β-carotene
Chl-*a*	chlorophyll-*a*
Cyt	cytochrome
DOPC	dioleoylphosphatidylcholine (neutral lipid)
DOPG	dioleoylphosphatidylglycerol (anionic lipid)
FNR	ferredoxin-NAD(P)$^+$-oxidoreductase
ISP	Rieske iron-sulfur protein
MGDG	monogalactosyldiacylglycerol (neutral lipid)
Mr	molecular weight
n,p-side	electrochemically negative and positive side of membrane
PA	phosphatidic acid (anionic lipid)
PG	phosphatidylglycerol (anionic lipid)
Q_p-site	quinol oxidation site
SQDG	sulfoquinovosyldiacylglycerol (anionic lipid)
Sub IV	subunit IV
TDS	tridecyl-stigmatellin
TMH	transmembrane helix
TNS	Tris-NaCl-sucrose buffer
UDM	n-Undecyl-β-D-maltopyranoside

References

1. Schutz M, Brugna M, Lebrun E, Baymann F, Huber R, Stetter KO, Hauska G, Toci R, Lemesle-Meunier D, Tron P, Schmidt C, Nitschke W. Early evolution of cytochrome bc complexes. Journal of molecular biology. 2000; 300:663–675. [PubMed: 10891261]
2. Darrouzet E, Cooley JW, Daldal F. The Cytochrome bc (1) Complex and its Homologue the b (6) f Complex: Similarities and Differences. Photosynth Res. 2004; 79:25–44. [PubMed: 16228398]
3. Widger WR, Cramer WA, Herrmann RG, Trebst A. Sequence homology and structural similarity between cytochrome b of mitochondrial complex III and the chloroplast b6-f complex: position of the cytochrome b hemes in the membrane. Proceedings of the National Academy of Sciences of the United States of America. 1984; 81:674–678. [PubMed: 6322162]
4. Cramer WA, Hasan SS, Yamashita E. The Q cycle of cytochrome bc complexes: a structure perspective. Biochimica et biophysica acta. 2011; 1807:788–802. [PubMed: 21352799]
5. Berry EA, Guergova-Kuras M, Huang LS, Crofts AR. Structure and function of cytochrome bc complexes. Annual review of biochemistry. 2000; 69:1005–1075.
6. Kurisu G, Zhang H, Smith JL, Cramer WA. Structure of the cytochrome b6f complex of oxygenic photosynthesis: tuning the cavity. Science. 2003; 302:1009–1014. [PubMed: 14526088]
7. Stroebel D, Choquet Y, Popot JL, Picot D. An atypical haem in the cytochrome b(6)f complex. Nature. 2003; 426:413–418. [PubMed: 14647374]
8. Yan JS, Kurisu G, Cramer WA. Intraprotein transfer of the quinone analogue inhibitor 2,5-dibromo-3-methyl-6-isopropyl-p-benzoquinone in the cytochrome b(6)f complex. Proceedings of the National Academy of Sciences of the United States of America. 2006; 103:69–74. [PubMed: 16371475]
9. Baniulis D, Yamashita E, Whitelegge JP, Zatsman AI, Hendrich MP, Hasan SS, Ryan CM, Cramer WA. Structure-Function, Stability, and Chemical Modification of the Cyanobacterial Cytochrome b6f Complex from Nostoc sp. PCC 7120. The Journal of biological chemistry. 2009; 284:9861–9869. [PubMed: 19189962]
10. Yamashita E, Zhang H, Cramer WA. Structure of the cytochrome b6f complex: quinone analogue inhibitors as ligands of heme cn. Journal of molecular biology. 2007; 370:39–52. [PubMed: 17498743]
11. Moser CC, Keske JM, Warncke K, Farid RS, Dutton PL. Nature of biological electron transfer. Nature. 1992; 355:796–802. [PubMed: 1311417]
12. Zhang Z, Huang L, Shulmeister VM, Chi YI, Kim KK, Hung LW, Crofts AR, Berry EA, Kim SH. Electron transfer by domain movement in cytochrome bc1. Nature. 1998; 392:677–684. [PubMed: 9565029]
13. Carrell CJ, Schlarb BG, Bendall DS, Howe CJ, Cramer WA, Smith JL. Structure of the soluble domain of cytochrome f from the cyanobacterium Phormidium laminosum. Biochemistry. 1999; 38:9590–9599. [PubMed: 10423236]
14. Martinez SE, Huang D, Szczepaniak A, Cramer WA, Smith JL. Crystal structure of chloroplast cytochrome f reveals a novel cytochrome fold and unexpected heme ligation. Structure. 1994; 2:95–105. [PubMed: 8081747]
15. Hasan SS, Cramer WA. On rate limitations of electron transfer in the photosynthetic cytochrome b(6)f complex. Phys Chem Chem Phys. 2012; 14:13853–13860. [PubMed: 22890107]
16. Zhang H, Kurisu G, Smith JL, Cramer WA. A defined protein-detergent-lipid complex for crystallization of integral membrane proteins: The cytochrome b6f complex of oxygenic photosynthesis. Proceedings of the National Academy of Sciences of the United States of America. 2003; 100:5160–5163. [PubMed: 12702760]
17. Zhang H, Cramer WA. Purification and crystallization of the cytochrome b6f complex in oxygenic photosynthesis. Methods in molecular biology. 2004; 274:67–78. [PubMed: 15187270]
18. Otwinowski Z, Minor W. Processing of X-ray diffraction data collected in oscillation mode. Method Enzymol. 1997; 276:307–326.
19. Murshudov GN, Skubak P, Lebedev AA, Pannu NS, Steiner RA, Nicholls RA, Winn MD, Long F, Vagin AA. REFMAC5 for the refinement of macromolecular crystal structures. Acta Crystallogr D. 2011; 67:355–367. [PubMed: 21460454]

20. Emsley P, Lohkamp B, Scott WG, Cowtan K. Features and development of Coot. Acta Crystallogr D. 2010; 66:486–501. [PubMed: 20383002]
21. Adams PD, Afonine PV, Bunkoczi G, Chen VB, Davis IW, Echols N, Headd JJ, Hung LW, Kapral GJ, Grosse-Kunstleve RW, McCoy AJ, Moriarty NW, Oeffner R, Read RJ, Richardson DC, Richardson JS, Terwilliger TC, Zwart PH. PHENIX: a comprehensive Python-based system for macromolecular structure solution. Acta crystallographica. Section D, Biological crystallography. 2010; 66:213–221.
22. Sobolev V, Sorokine A, Prilusky J, Abola EE, Edelman M. Automated analysis of interatomic contacts in proteins. Bioinformatics. 1999; 15:327–332. [PubMed: 10320401]
23. Zhang H, Whitelegge JP, Cramer WA. Ferredoxin:NADP+ oxidoreductase is a subunit of the chloroplast cytochrome b6f complex. The Journal of biological chemistry. 2001; 276:38159–38165. [PubMed: 11483610]
24. Gounaris K, Barber J, Harwood JL. The thylakoid membranes of higher plant chloroplasts. The Biochemical journal. 1986; 237:313–326. [PubMed: 3541898]
25. Gounaris K, Andersson CSB, Barber J. Lateral heterogeneity of polar lipids in the thylakoid membranes of spinach chloroplasts. FEBS letters. 1983; 156:170–174.
26. Crofts AR, Guergova-Kuras M, Huang L, Kuras R, Zhang Z, Berry EA. Mechanism of ubiquinol oxidation by the bc(1) complex: role of the iron sulfur protein and its mobility. Biochemistry. 1999; 38:15791–15806. [PubMed: 10625445]
27. Hasan SS, Yamashita E, Ryan CM, Whitelegge JP, Cramer WA. Conservation of lipid functions in cytochrome bc complexes. Journal of molecular biology. 2011; 414:145–162. [PubMed: 21978667]
28. de Vitry C, Ouyang Y, Finazzi G, Wollman FA, Kallas T. The chloroplast Rieske iron-sulfur protein. At the crossroad of electron transport and signal transduction. The Journal of biological chemistry. 2004; 279:44621–44627. [PubMed: 15316016]
29. Lange C, Nett JH, Trumpower BL, Hunte C. Specific roles of protein-phospholipid interactions in the yeast cytochrome bc1 complex structure. The EMBO journal. 2001; 20:6591–6600. [PubMed: 11726495]
30. Palsdottir H, Hunte C. Lipids in membrane protein structures. Biochimica et biophysica acta. 2004; 1666:2–18. [PubMed: 15519305]
31. Jones MR. Lipids in photosynthetic reaction centres: structural roles and functional holes. Progress in lipid research. 2007; 46:56–87. [PubMed: 16963124]
32. Aoki M, Sato N, Meguro A, Tsuzuki M. Differing involvement of sulfoquinovosyl diacylglycerol in photosystem II in two species of unicellular cyanobacteria. European journal of biochemistry / FEBS. 2004; 271:685–693. [PubMed: 14764084]
33. Sato N. Roles of the acidic lipids sulfoquinovosyl diacylglycerol and phosphatidylglycerol in photosynthesis: their specificity and evolution. Journal of plant research. 2004; 117:495–505. [PubMed: 15538651]
34. Minoda A, Sato N, Nozaki H, Okada K, Takahashi H, Sonoike K, Tsuzuki M. Role of sulfoquinovosyl diacylglycerol for the maintenance of photosystem II in Chlamydomonas reinhardtii. European journal of biochemistry / FEBS. 2002; 269:2353–2358. [PubMed: 11985618]
35. Fromme P, Jordan P, Krauss N. Structure of photosystem I. Bba-Bioenergetics. 2001; 1507:5–31. [PubMed: 11687205]
36. Grotjohann I, Fromme P. Structure of cyanobacterial photosystem I. Photosynth Res. 2005; 85:51–72. [PubMed: 15977059]
37. White SH, Wimley WC. Membrane protein folding and stability: physical principles. Annual review of biophysics and biomolecular structure. 1999; 28:319–365.
38. Yan J, Cramer WA. Functional insensitivity of the cytochrome b6f complex to structure changes in the hinge region of the Rieske iron-sulfur protein. The Journal of biological chemistry. 2003; 278:20925–20933. [PubMed: 12672829]
39. Solmaz SR, Hunte C. Structure of complex III with bound cytochrome c in reduced state and definition of a minimal core interface for electron transfer. The Journal of biological chemistry. 2008; 283:17542–17549. [PubMed: 18390544]

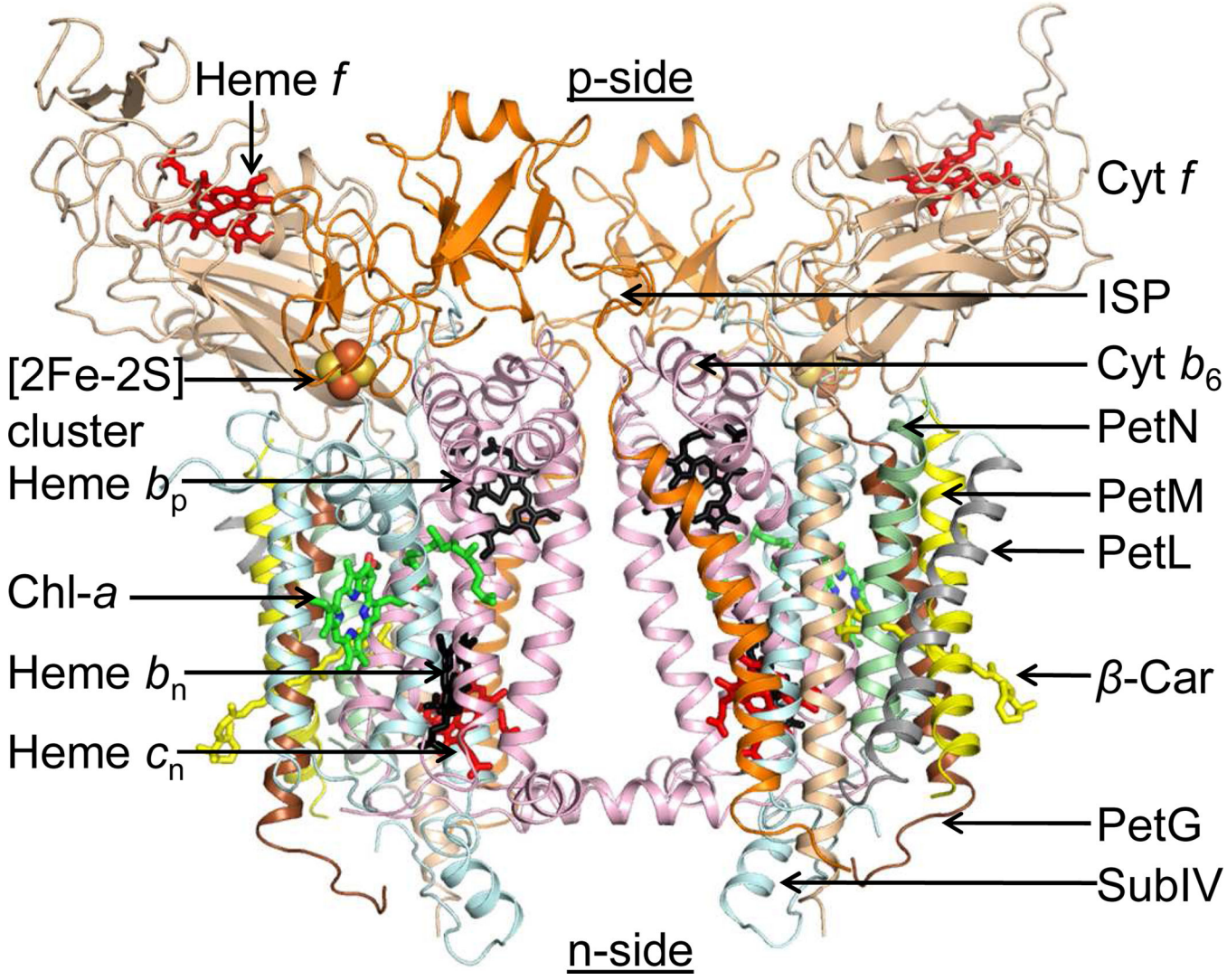

Fig 1.

Cyt b_6f complex from the moderately thermophilic cyanobacterium *Mastigocladus laminosus* (PDB ID 2E74). Polypeptide subunits are shown as ribbons and prosthetic groups as sticks and spheres. Color scheme: Cytochrome b_6 (cyt b_6), pink; subunit IV (sub IV), cyan; cytochrome *f* (cyt *f*), wheat; Iron-Sulfur Protein (ISP), orange; Pet G, brown; Pet L, gray; Pet M, yellow; Pet N, green.

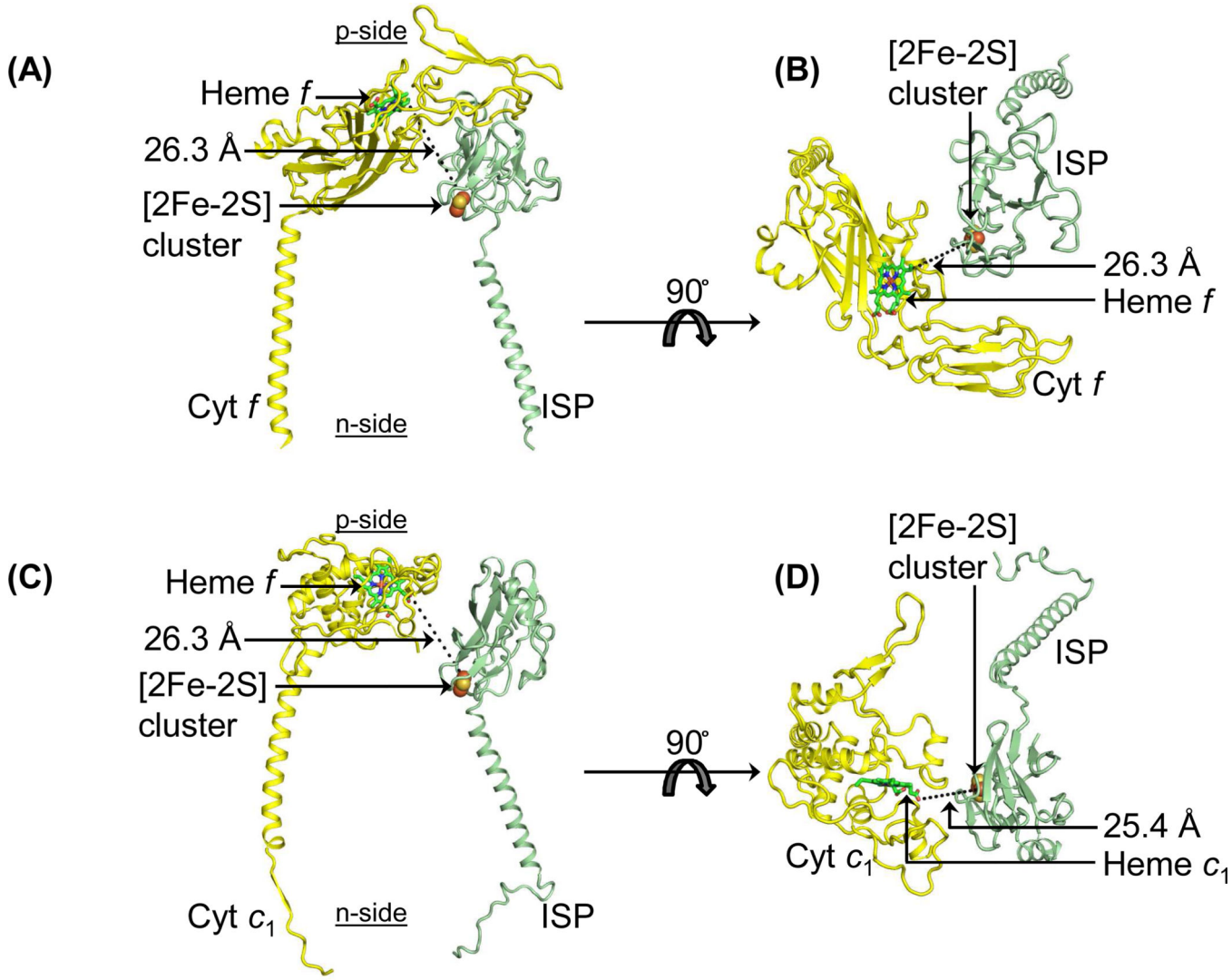

Fig 2.

p-Side extrinsic domain architecture of the cyt b_6f (PDB ID 2E74) and bc_1 complex (PDB ID 3CX5). (**A, B**) The cyt *f* extrinsic domain (yellow) consists of an elongated β–sheet structure that extends over 75 Å1. (**C, D**) In contrast, the cyt c_1 extrinsic domain (yellow) is predominantly α–helical in structure and is more compact. The ISP polypeptide is shown in pale green, the heme of cyt *f*/cyt c_1 in green/red (sticks) and the ISP [2Fe-2S] cluster as brown/wheat spheres.

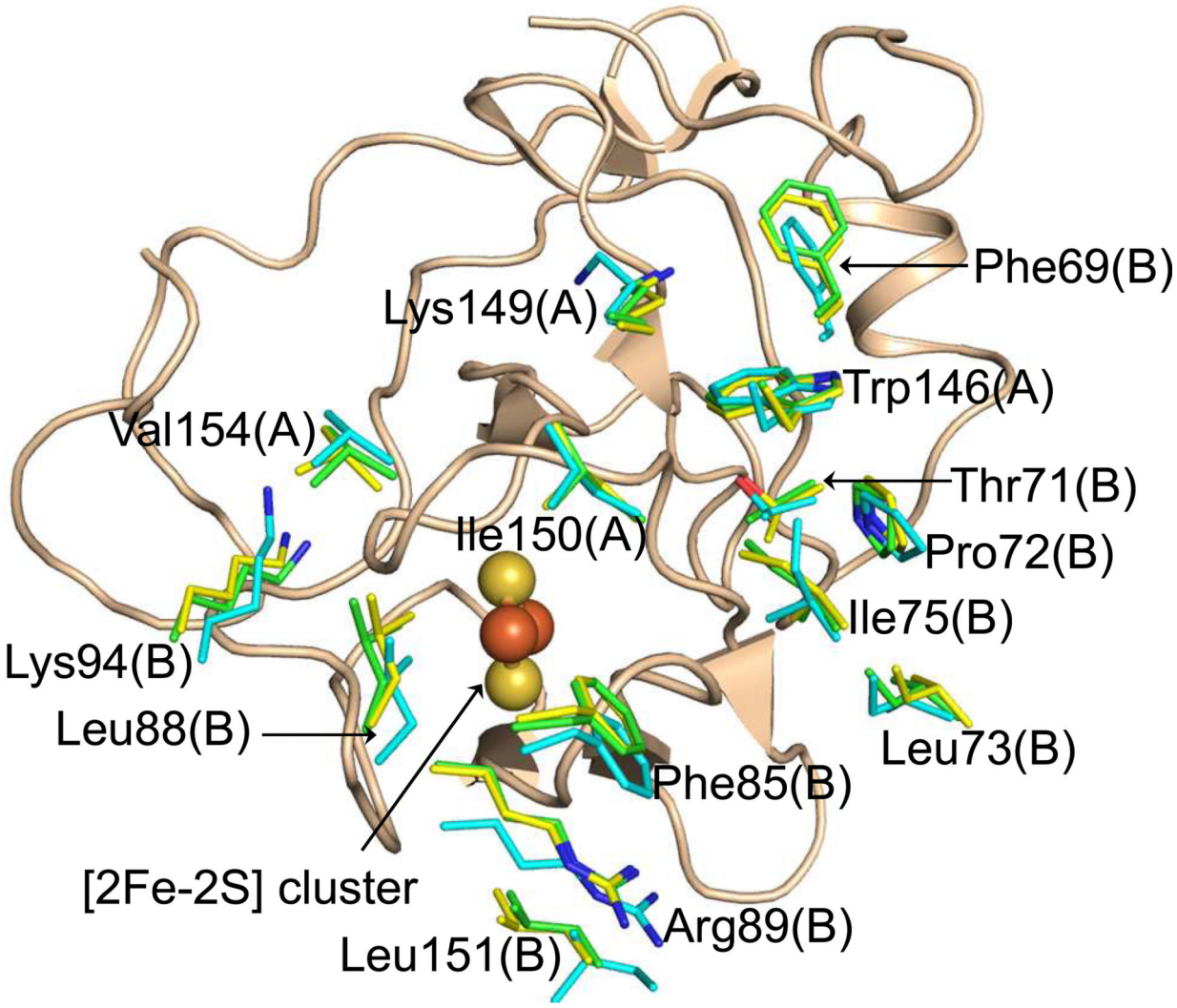

Fig 3.

Docking interface for ISP extrinsic domain. The figure was generated by superposition of three crystal structures of the cyt b_6f complex- PDB IDs 2E74, 2E76 and 4I7Z (described in present study). Residues from cyt b_6 are identified as "**A**" and those of sub IV by "**B**". The ISP extrinsic domain is shown as wheat colored ribbon and includes the [2Fe-2S] cluster. Residues are color coded according to their respective crystal structures- PDB ID 2E74 (yellow), PDB ID 2E76 (cyan) and PDB ID 4I7Z (green). No large conformational changes are observed in the ISP docking interface.

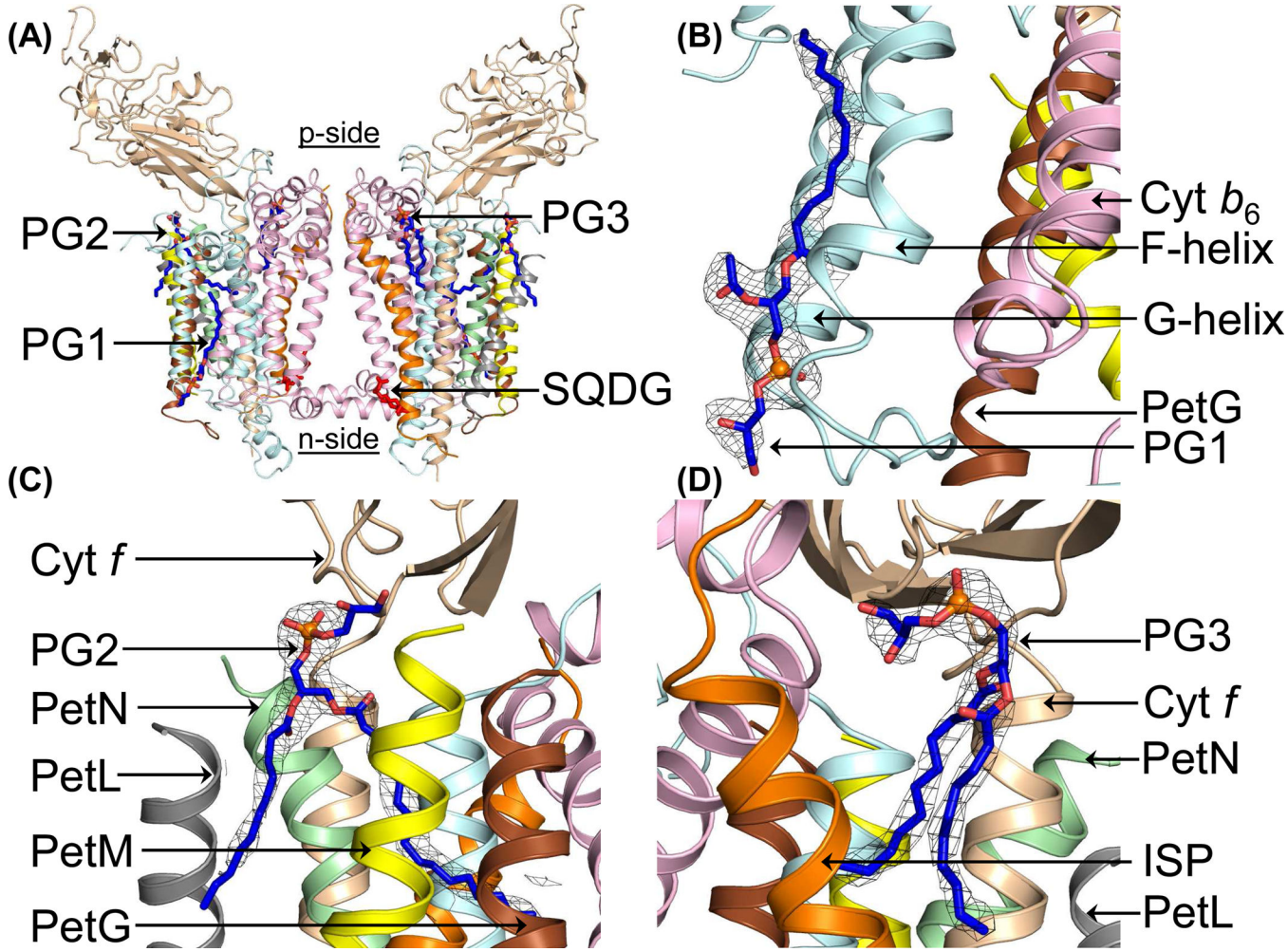

Fig 4.

Anionic lipid binding sites in cyt b_6f. (**A**) Four anionic lipid sites in the b_6f complex. (**B**) PG1 bound between the F and G TMH of sub IV. (**C**) PG2 inserted between peripheral Pet subunits. (**D**) PG3 located between ISP and cyt *f* TMH. Mesh, 2Fo-Fc map, 1.2 σ. Color code same as in Fig. 1.

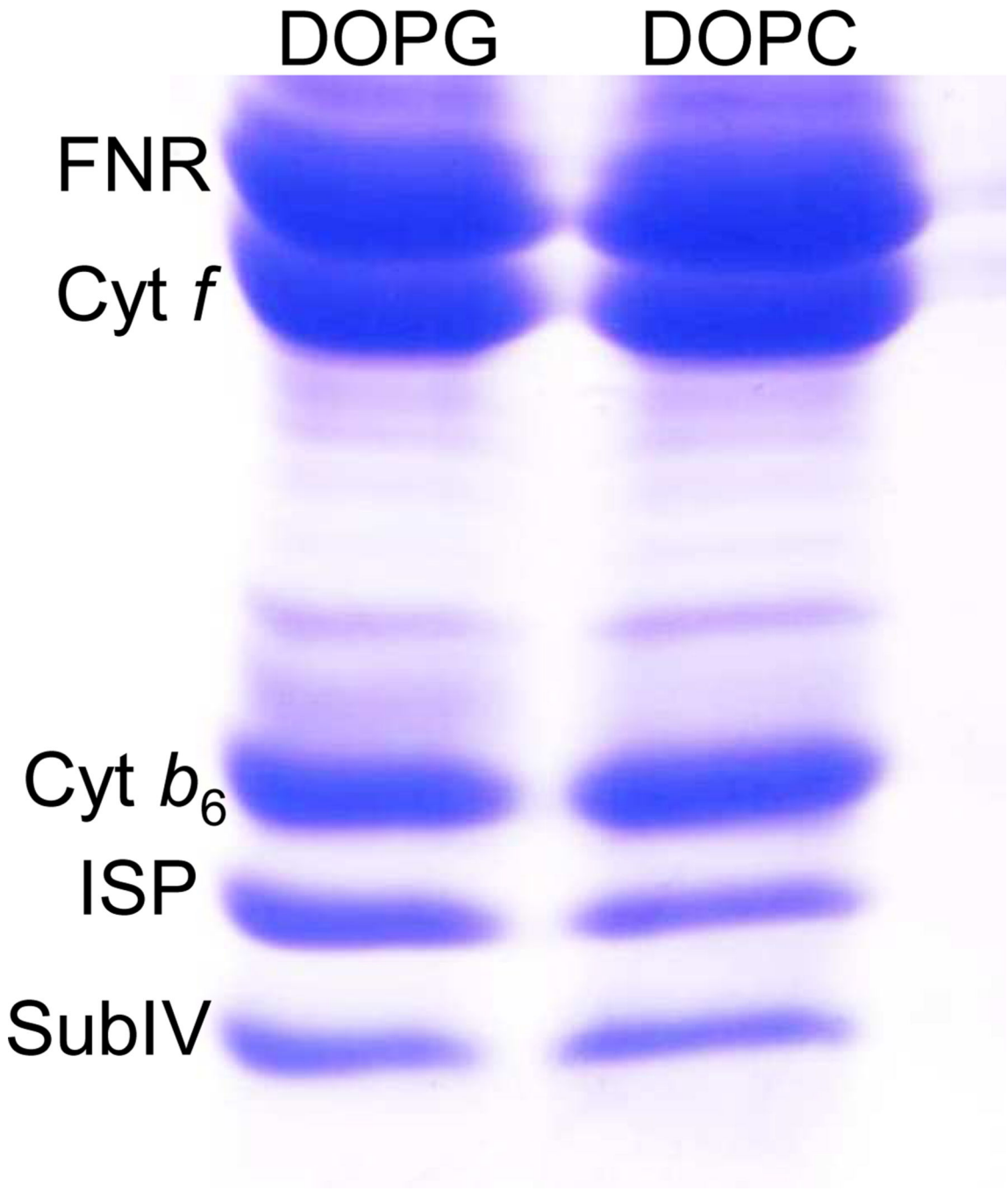

Fig 5.

Lipid-dependence of stability of purified cyt b_6f complex in lipids. Purified cyt b_6f complex from spinach thylakoid membranes was reconstituted with lipids (DOPG or DOPC) at a molar ratio (protein:lipid) of 1:10. The molecular mass of the ISP subunit does not undergo a change in the presence of the anionic lipid DOPG thereby indicating that the polypeptide remains intact in the presence of the anionic lipid. The band for the enzyme FNR, which co-purifies with the spinach cyt b_6f complex, is also shown.

Table 1

Crystallographic data summary (data merged from two crystals; values in parentheses correspond to outer shell)

Crystal	**Cyt b_6f with DOPG**
Data Collection	
Space Group	$P6_122$
a, *b*, *c* (Å)	159.45, 159.45, 362.75
α, β, γ(Å)	90, 90, 120
Resolution (Å)	50.00–2.80 (2.85–2.80)
R_{merge}	0.12 (0.45)
$\langle I \rangle / \langle \sigma_I \rangle$	15.6 (2.1)
Completeness (%)	99.2 (94.7)
Redundancy	9.3 (4.3)
Refinement	
Resolution (Å)	48.52–2.80
Reflections	627305
R_{work}/R_{free}	0.247/0.271
RMS Deviation	
Bond lengths (Å)	0.003
Bond angles (°)	0.931